HHS Public Access

Author manuscript

Environ Geochem Health. Author manuscript; available in PMC 2018 September 09.

Published in final edited form as:

Environ Geochem Health. 2018 October ; 40(5): 1785–1802. doi:10.1007/s10653-017-9926-5.

Oxidative potential (OP) and mineralogy of iron ore particulate matter at the Gol-E-Gohar Mining and Industrial Facility (Iran)

Naghmeh Soltani,
Department of Earth Sciences, College of Science, Shiraz, University, Shiraz 71454, Iran

Behnam Keshavarzi,
Department of Earth Sciences, College of Science, Shiraz, University, Shiraz 71454, Iran

Armin Sorooshian,
Department of Chemical and Environmental Engineering, University of Arizona, Tucson, AZ 85721, USA. Department of Hydrology and Atmospheric Sciences, University of Arizona, Tucson, AZ 85721, USA

Farid Moore,
Department of Earth Sciences, College of Science, Shiraz, University, Shiraz 71454, Iran

Christina Dunster,
MRC-PHE Centre for Environment and Health, King's College London, 150 Stamford Street, London SE1 9NH, UK

Ana Oliete Dominguez,
MRC-PHE Centre for Environment and Health, King's College London, 150 Stamford Street, London SE1 9NH, UK

Frank J. Kelly,
MRC-PHE Centre for Environment and Health, King's College London, 150 Stamford Street, London SE1 9NH, UK

Prakash Dhakal,
Department of Soil, Water and Environmental Science, University of Arizona, Tucson, AZ 85721, USA

Mohamad Reza Ahmadi, and
Gol-E-Gohar Iron Ore and Steel Research Institute, Gol-E-Gohar Mining and Industrial Co., Sirjan, Iran

Sina Asadi
Department of Earth Sciences, College of Science, Shiraz, University, Shiraz 71454, Iran

Abstract

Correspondence to: Naghmeh Soltani.

Electronic supplementary material The online version of this article (doi:10.1007/s10653-017-9926-5) contains supplementary material, which is available to authorized users.

Concentrations of total suspended particulate matter, particulate matter with aerodynamic diameter <2.5 μm ($PM_{2.5}$), particulate matter <10 μm (PM_{10}), and fallout dust were measured at the Iranian Gol-E-Gohar Mining and Industrial Facility. Samples were characterized in terms of mineralogy, morphology, and oxidative potential. Results show that indoor samples exceeded the 24-h $PM_{2.5}$ and PM_{10} mass concentration limits (35 and 150 μg m^{-3}, respectively) set by the US National Ambient Air Quality Standards. Calcite, magnetite, tremolite, pyrite, talc, and clay minerals such as kaolinite, vermiculite, and illite are the major phases of the iron ore PM. Accessory minerals are quartz, dolomite, hematite, actinolite, biotite, albite, nimite, laumontite, diopside, and muscovite. The scanning electron microscope structure of fibrous-elongated minerals revealed individual fibers in the range of 1.5 nm to 71.65 μm in length and 0.2 nm to 3.7 μmin diameter. The presence of minerals related to respiratory diseases, such as talc, crystalline silica, and needle-shaped minerals like amphibole asbestos (tremolite and actinolite), strongly suggests the need for detailed health-based studies in the region. The particulate samples show low to medium oxidative potential per unit of mass, in relation to an urban road side control, being more reactive with ascorbate than with glutathione or urate. However, the PM oxidative potential per volume of air is exceptionally high, confirming that the workers are exposed to a considerable oxidative environment. PM released by iron ore mining and processing activities should be considered a potential health risk to the mine workers and nearby employees, and strategies to combat the issue are suggested.

Keywords

Particulate matter; Amphibole asbestos; Oxidative potential; Iron ore; Mining

Introduction

A broad spectrum of earth materials has been linked to, blamed for, and/or debated as sources for disease. Excessive exposure to mineral dusts has long been recognized for promoting diseases such as those linked to asbestos (asbestosis, mesothelioma, lung cancer), silica dust (silicosis, lung cancer), and coal dust (coal-worker pneumoconiosis) (Plumlee et al. 2006; Singh et al. 2009). The health effects of exposure to particulate matter emitted from surface mining and processing operation are well documented and remain a major issue (Hendryx 2009; Lal and Tripathy 2012; Love et al. 1997; Stafilov et al. 2010). Lung cancer is a common disease among workers who are exposed to iron ore dust (Boyd et al. 1970; Chau et al. 1993; Chen et al. 1990; Kinlen and Willows 1988; Wild et al. 2009).

Amphibole asbestos can develop in iron ore mines and related processing facilities, causing respiratory diseases (Berndt and Brice 2008; Brunner et al. 2008; Clemente et al. 2007; Park and Wexler 2008; Ross et al. 2008). Asbestos fibers include microscopic fibers either in the form of serpentine threads (curly stranded structures) or amphibole fibers (straight, rod-like fibers) (Bhattacharjee and Paul 2016). Research has shown that the serpentine-like “chrysotile” is most abundant, whereas the amphibole fibers are more bio-persistent (Kamp and Weitzman 1999; Liu et al. 2013). Phagocytic cells attack foreign objects, such as asbestos fibers, by engulfing and ultimately removing them. This process produces highly reactive compounds, such as hydrogen peroxide and hydroxyl radicals. This production is

promoted by the presence of ferrous iron that ultimately increases inflammation in the area of the fiber and may cause DNA damage in the surrounding cells (Eby 2004). Measurements of air pollutants arising from open-pit mining and processing operations include total suspended particulate matter with an equivalent aerodynamic diameter of 30 μm and above (TSP) (Patra et al. 2016) and particles with an equivalent aerodynamic diameter smaller than 10 μm (PM_{10}) and 2.5 μm ($PM_{2.5}$) (Chakraborty et al. 2002; Sinha and Banerjee 1997). Within these categories of PM, measurements are taken for aerosol properties considered to be critical from a health and safety perspective, including chemical composition, shape, and dust mass concentration (Meyer et al. 1996). An understanding of mineral chemistry and crystal structure is also important (Eby 2004). These detailed measurements are of importance for medical scientists who can then advise about medical problems involving geomaterials and biominerals (Sahai et al. 2006).

Adverse health outcomes associated with exposure to fine ($PM_{2.5}$) and ultrafine particles have been attributed to oxidative stress on particles caused by the presence of reactive oxygen species (ROS) and generation of both free radicals and related ROS at their sites of deposition (Dellinger et al. 2001; Li et al. 2003; Nel 2005). Oxidative stress caused by ROS has been suggested as an important underlying mechanism of action by which exposure to PM may lead to adverse health effects (Chuang et al. 2013; Dellinger et al. 2001; Li et al. 2003; Nel 2005). The oxidative potential (OP), defined as a measure of the capacity of PM to oxidize target molecules, is more closely related to biological responses to PM exposures as compared to PM mass alone (Borm et al. 2007). Oxidative potential includes various biologically relevant properties of PM, including size, surface, mineral, and chemical composition (Janssen et al. 2014). Of note is that transition metals such as iron, copper, and vanadium and organic chemical species found in particulate matter at relatively low concentrations are likely to contribute significantly to oxidative potential and subsequent toxicity by initiating ROS formation both directly and indirectly through redox-mediated mechanisms (Fantel 1996; Kelly et al. 2011; Valko et al. 2005).

Recent growth in mining and mineral processing activities in the Gol-E-Gohar (GEG) mine, located in southern Iran, has resulted in increased emissions of particulate matter (PM) and associated contaminants. As a result of scarcity of water in the region, the dry grinding method is employed leading to strong dust emissions. At this company, approximately 3000 employees are working, many of which are mine workers directly exposed to iron ore particulate matter. Addressing health effects of emitted aerosol requires a characterization of properties, such as chemical composition, shape, dust mass concentration, mineral chemistry, and crystal structure (Eby 2004; Meyer et al. 1996; Sinha and Banerjee 1997).

Previous studies conducted at GEG were directed at understanding mineralization (Babaki and Aftabi 2006; Heydari 2008; Mücke and Golestaneh 1982), mineralogy and petrography (Mücke and Younessi 1994), mining method of the ore bodies (Azadeh et al. 2010; Saeidi et al. 2014), environmental impact assessment (Phillips 2013), and groundwater characteristics (Jahanshahi and Zare 2015). However, no research has been documented about PM mineralogy and associated health effects around GEG. The present study has two major goals: (1) comprehensively characterize the morphology and mineralogy of PM and fallout dust from GEG mining and processing activities; and (2) estimate oxidative potential (OP)

of these particles to address the mechanisms by which PM impacts the respiratory tract lining fluid (RTLF) antioxidant network and to identify those components driving the observed effects.

Materials and methods

Study area

The Gol-E-Gohar (GEG) iron deposit is located 55 km southwest of Sirjan city in the Kerman Province, Iran (Fig. 1). Structurally, the GEG iron deposit is located on the eastern edge of the Sanandaj-Sirjan magmatic-metamorphic zone (SSZ) and in the foreland of the Zagros Ranges in an area of planar desert topography (Alavi 2004; Mücke and Younessi 1994). The study area can be classified as having simultaneous mining, processing, and tailing activities.

The GEG iron deposit is characterized by six separate ore bodies with a total area of 40 km^2. It is one of the most important economic iron deposits in Iran, and the total reserve of iron is estimated to be more than 1135 Mt. at a grade of about 57.2% Fe, 0.16% P, and 1.86% S (Hosseini and Asghari 2016; Mirnejad et al. 2011; Nabatian et al. 2015).

The geology of the region is characterized by Paleozoic metamorphic rocks, Mesozoic and Cenozoic sedimentary rocks, and Quaternary deposits (Mücke and Younessi 1994). The host rocks of the iron ore deposit include metamorphosed volcanic ± sedimentary rocks of the greenschist facies, probably of Lower Paleozoic age (Saeidi et al. 2014). The characteristics of the Fe-rich hosts as products of replacement, the distinctive geochemical signatures, alteration styles, and geochronological data all point to an epigenetic hydrothermal origin and classification as an iron oxide copper gold (IOCG) deposit in the GEG area (Williams et al. 2005). The deposit consists mostly of metamorphic rocks such as mica-schist, amphibolite, quartz-schist, calcitic and dolomitic marbles, and quartzite. These rock units are strongly folded and might have been metamorphosed in Late Paleozoic and Early Mesozoic. The metamorphic rocks are highly tectonized (Babaki and Aftabi 2006; Sabzehei et al. 1997). The mineralized zone has a vertical zonation from top to bottom which are top magnetite, oxide zone, and bottom magnetite (Saadat et al. 2014; Sabzehei et al. 1997).

In the GEG deposit, magnetite, pyrite, pyrrhotite, chalcopyrite, pentlandite, and sphalerite are the main ore minerals. Massive and brecciated magnetite is accompanied by apatite and is locally martitized. Alteration minerals such as actinolite, olivine, hornblende, phlogopite, chlorite, and carbonates are associated with the Fe-oxide minerals (Nabatian et al. 2015).

Other non-magnetic phases, including carbonates (e.g., calcite, dolomite, siderite), and silicates (e.g., quartz, talc, albite, tremolite, actinolite, muscovite, biotite, chlorite, kaolinite, vermiculite, illite) must be removed by ore refining processes.

The operation in this mine is an open-pit facility (Monjezi et al. 2009). Currently, 3 of 6 ore bodies are under mining and processing. Mine#1 is the largest one and produces up to 5 Mt. of ore per year and can be mined at that rate for decades. After removing overburden materials above the ore deposit, ore is transported to downstream processing site. Iron ore

processing plants such as concentrate plant (ICP), iron ore pelletizing plant (IPP), polycom plant (PLY), and hematite recovery plant (HRP) produce 6.1, 5.5, 2, and 1.2 million tons of iron ore concentrate per year, respectively.

The climate of the studied area, according to data between 2000 and 2014 from the Meteorological Organization of Iran (I.R. of Iran Meteorological organization, IRIMO, Sirjan Synoptic weather station), is arid with an annual average precipitation of 115 mm with more intense precipitation during the winter. The annual average air temperature is 18.1 °C and lies between an averages of −9.2 °C in the cold season (January) to 39.8 °C in the warm season (July). The dry period lasts from May to October. The prevailing wind direction is from the northeast. Natural vegetation in the region is mainly composed of sporadic shrubs and steppes.

Sampling

A total of 60 PM samples (see Supplemental Material, Table S1) were collected between December 17 2014 and May 21 2015 from ten different sites in the GEG complex (Fig. 1). These samples included 20 of $PM_{2.5}$, 20 of PM_{10}, and 20 of TSP. Additionally, 10 fallout dust (FD) and 15 rock (R) samples were obtained. As shown in Fig. 1, six of these sites were indoors, including two Iron Ore Pelletizing Plants (IPP_1 and IPP_2), in which magnetite grains were sorted from other minerals using large magnetic separators and then combined with other agents (binders and possible fluxing agents) and heated to high temperatures (1200–1500 °C) to create magnetite pellets. IPP_1 and IPP_2 represent areas before and after the furnace unit, respectively. Other indoor samples were collected in the Primary Crusher (PC), the Polycom Plant (PLY), the Hematite Recovery Plant (HRP), and the Iron Ore Concentration Plant (ICP). The four outdoor sampling areas included the Tail Bin (TB), outside of the Research and Development Center (R&D Center), the Mining Operation Office (MOO), and an official building named Building Number 45 (B No.45). The outdoor samples were collected near the main entrance doors owing to high staff traffic flow.

Fallout dust samples weighing ~500 g were collected with a plastic hand broom and transferred to a clean, self-sealed polyethylene bag. In the laboratory, samples were first air-dried at room temperature and then mechanically passed through a 2-mm nylon sieve to remove larger-sized particles. The samples were fractionated through a 220 mesh (63 μm) for particle size analysis and then homogenized in an agate mortar. A representative set of samples (N = 15 rock) for mineralogical studies of the GEG iron ores was collected during the field work. The rock samples are collected by the three different drill cores from the three exploratory wells (#0047, 0052, and 0068) of the iron ore at mine#1. The location description of the three exploratory wells is presented in Table S2. The rock samples were collected from well#0047 (from 38.6 to 40.6 m and 94.6–100.6 m in depth = 5 samples), well#0052 (23.2–29.2 m depth = 4 samples), and well#0068 (36.1–42.1 m depth = 6 samples). The three selected wells were chosen based on the fact that they cover the three main mineralized zones (top magnetite, oxide zone, and the bottom magnetite) at the mine. The wells also had a suitable distance from each other.

PM samples were collected on Teflon (PTFE) filter papers (46.2 mm in diameter, 2 μm pore size, with support ring, Tisch Scientific, USA) using an ECHO PM ambient filter sampler

(TECORA, Italy). The dust collection system comprises a low-volume sampler unit (LVS) and a filter changer with an intake tube and sampling head (inlet) to collect particulate matter from indoor and outdoor air. Air is drawn through a size-selective inlet and through filter media. Particulates with aerodynamic diameters less than the cut-point of the inlet are collected on the filter media. The sampling inlet of the instrument used for sampling was set up at a height of 120 cm corresponding to the breathing zone of the workers. The sampling flow rate was 16.67 L min^{-1} (i.e., 1 m^3 h^{-1}) in accordance with the reference methods US EPA 40 CFR part 50 for PM_{10} and $PM_{2.5}$ (EPA 2006). Before sampling, filters were pre-conditioned in a desiccator at 25 °C and 25% relative humidity for 24 h, and then weighed. After PM sampling, all filters were conditioned in an air-tight desiccation chamber for 24 h and then re-weighed for a quantitative measurement (by difference) of bulk mass of collected PM on the filters. Filters were kept in plastic petri dishes sealed with parafilm and stored at 4 °C until oxidative potential and mineralogical analysis. A minimum of one field blank filter was also obtained for every 10 samples during the complete sampling campaign and treated by the same procedures for loaded filters. Only one field blank was taken for oxidative potential assay.

Analysis

Gravimetric analysis—Particulate concentrations ($N = 60$) were measured gravimetrically (Table S3) using the standard procedure of differential weighing of a filter before and after exposure to a constant air flow for 24 h (USEPA 1999). PTFE filters were weighed using an electron analytical microbalance (Model LIBROR AEL-40SM; SHI-MADZU Co., Kyoto, Japan) with a 1-μg sensitivity after being equilibrated for 24 h in a silica gel desiccator at a constant condition at 20 ± 1 °C and 20 ± 5% relative humidity to eliminate interfering factors (e.g., humidity) in PM measurements. Filters were handled with Teflon tape-coated tweezers to reduce the possibility of contamination. It is assumed that PM deposited on filter substrates were uniformly distributed over the entire area. Standard operating procedures were employed to validate the gravimetric measurements of $PM_{2.5}$, PM_{10}, and TSP mass concentrations, including flow rate calibration and the use of field and laboratory blank filters (Amato et al. 2009; EPA 2006; Szigeti et al. 2014).

Mineralogical analysis—A series of microscopy and analytical techniques were utilized to identify the presence and physical and geochemical characteristics of the collected samples. These techniques are summarized below.

Characterization and quantification of PM using X-ray diffraction (XRD): Mineralogical composition (%) of PM and fallout dust was analyzed using X-ray diffraction (XRD) where bulk semi-quantitative analysis was performed using full XRD pattern fit Rietveld refinement method (Bish and Post 1993; Bish 1994), an extension of the Rietveld method (Rietveld 1969). Semi-quantitative XRD analysis is a qualitative method to obtain bulk mineralogical composition of the sample, and QXRD analysis provides percent mineralogical composition within ≤4% of the weight percents at the 95% confidence level. Additionally, sample preparation, and uncertainty of Rietveld and Rockjock methods have been discussed elsewhere (Bish and Post 1993; Chipera and Bish 2013; Bish 1994). In

addition, to evaluate the reliability of the quantitative results from XRD data, the goodness-of-fit (GOF) factors (X^2) for samples are monitored in the caption of XRD graphs.

Quantitative XRD (QXRD) of three PM samples (SP_1, SP_{12}, and SP_{43}) was performed using combination of the Rietveld method and the Rockjock method (Eberl 2003) at the University of Arizona's Center for Environmental Physics and Mineralogy using a PANalytical X'Pert PRO Multi-Purpose Diffractometer (PANalytical, Almelo, The Netherlands). The system generated Cu-Kα X-rays at an accelerating potential of 45 kV and current of 40 mA. A spinner sample stage with a 4-s rotation time was used to measure from 5 to 65° 2-θ, with a step size of 0.020° and a dwell time of 1.25 s. For quantitative analysis, air-dried samples were ground in a McCrone micronizing mill with the addition of 20% corundum internal standard (Eberl 2003). The addition of corundum as an internal standard allows precise mineral percent quantification.

Similarly, semi-quantitative mineral assemblage in the bulk samples (SP_4, SP_5, SP_{10}, SP_{31}, D_1, D_2, D_5, and D_{10}) was determined in the 5 to 65° (2-θ) range. For bulk mineral semi-quantitative analysis, air-dried representative samples were analyzed as collected without treatment. Both bulk and quantitative samples were prepared as bottom packed random powder mounts on a spinner disk and analyzed by XRD.

Microscopy and spectroscopy analysis: Thin-polished sections from the ten fallout dust (FD) samples (D_1–D_{10}) and 15 rock samples (R_1–R_{15}) were prepared and analyzed in a PLM for mineral observation. This analysis was carried out using an Olympus System Microscope (Model BX41TF, Reflected/Transmitted Polarizing Light Microscope, Japan) in the mineralogical laboratory at Shiraz University.

Scanning electron microscopy (SEM) attached with an energy-dispersive X-ray spectroscopy (EDS) was another technique used to analyze nine samples (D_1, D_2, D_5, D_{10}, SP_1, SP_5, SP_{10}, SP_{12}, and SP_{25}).

The SEM/EDS technique allows for a semi-quantitative elemental analysis (with the EDS unit) after a high-resolution particle morphology analysis (with the SEM). A small amount was used from each sample (approximately 0.005 g) and placed in the SEM microscope chamber. The SEM/EDS analysis was carried out with a SEM model S-3400 N Fully Automated Variable Pressure with magnification ranging from 5 to 300000×, in the University Spectroscopy and Imaging Facility (USIF) of the University of Arizona. The operating conditions were as follows: resolution of 3.0 nm (at 30 kV, secondary electron image, high vacuum) and scattered using BSE detector.

Oxidative potential—Oxidative potential of PM samples ($N = 29$) was assessed by antioxidant depletion using a synthetic respiratory tract lining fluid (RTLF) model. The RTLF model, developed by Zielinski et al. (1999), has been used previously to evaluate the toxicity of a variety of PM samples (Künzli et al. 2006; Mudway et al. 2004). It is based on the interaction of PM with three antioxidants commonly found on the surface of the lung, ascorbic acid (AA), urate (UA), and reduced glutathione (GSH), which are sensitive to intrinsic redox active PM constituents such as transition metals and quinones (Godriet al.

2010a; Szigeti et al. 2014). It contains no lung tissue or cells (Kelly et al. 2011). The RTLF model is more reflective of a healthy lung scenario (Shi et al. 2003; Zielinski et al. 1999).

Iron ore PM sample extracts were resuspended in 2% MeOH in water and were analyzed in triplicate. In a total volume of 0.5 mL, 50 μg PM mL^{-1} was incubated for 4 h at 37 °C with a synthetic RTLF solution containing equimolar concentrations (200 μmol L^{-1}) of ascorbic acid (AA), urate (UA), and reduced glutathione (GSH). To eliminate as much background antioxidant oxidation as possible from the model system, HPLC-grade water (pH 7.0) that had been treated previously with Chelex-100 resin (Sigma, UK) was used throughout for preparation of stocks and dilutions. Immediately following the 4-h incubation, samples were centrifuged and processed for analysis of the remaining antioxidants. A London roadside sample (LDN) was also included in the experiments to allow for qualitative comparison.

For quality control purposes, in-house controls of (i) particle-free, and two certified materials, namely (ii) M120, a negative PM (a generous gift from the Cabot Corporation, USA) and (iii) NIST1648a, an urban dust and a positive PM (NIST, USA) were incubated in parallel with the iron ore PM to control for background antioxidant after a 4-h incubation, assessment of the expected oxidation by the −ve and +ve controls in the RTLF exposure model, and for checks of cross-contamination from the processing of the PM. With a starting concentration of 200 μmol L^{-1} antioxidant (C_0), the remaining antioxidant concentrations after a 5-h incubation of the in-house controls were as expected. The −ve control PM (M120) displayed no reactivity with the antioxidant, whereas the +ve control PM (NIST1648a) displayed approximately 50% consumption of AA. A comparative London roadside sample (LDN) displayed the expected reactivity with the antioxidants.

Determination of glutathione: This assay employs the technique of the GSSG reductase-DTNB linked assay based on the method of Baker et al. (1990). 16.7 μL of the centrifuged RTLF-exposed liquid was added to 983.3 μL of cold 100 mM sodium phosphate buffer pH 7.5 containing 1 mM EDTA. Each diluted sample is analyzed in duplicate, using a microplate reader (Spectramax 190; Molecular Devices, UK), in parallel with glutathione standards. Total glutathione (GSX) and oxidized (GSSG) glutathione (via derivatization with 2-vinyl pyridine) are measured. The reduced (GSH) glutathione was obtained by subtracting the GSSG value from the GSX. The coefficient of variation (% CV) of analysis was less than 10% with a minimum detection limit of 0.3 μmol GSSG L^{-1}.

Determination of ascorbate (AA) and urate (UA): AA and UA were quantified by high-performance liquid chromatography (HPLC, Gilson Scientific UK; 150 × 4.6 mm 5 μm SphereClone ODS (2) column, Phenomenex, UK; electrochemical detector), using the method of Iriyama et al. (1984) with modifications. 50 μL of the centrifuged RTLF-exposed liquid was added to 450 μL of cold 5.6% meta-phosphoric acid, injected in the HPLC, and eluted with a 0.2 mol L^{-1} K_2HPO_4-H_3PO_4 (pH 2.1) mobile phase containing 0.25 mmol L^{-1} octanesulfonic acid. Final concentrations for AA and UA were calculated with external AA/UA standards, which were run simultaneously. The % CV of analysis was less than 5% with a minimum detection limit for ascorbic acid of 0.5 μmol L^{-1} and uric acid of 0.1 μmol L^{-1}. All chemicals were of the highest grade possible, usually HPLC-grade, and purchased from either the Sigma Chemical Company (UK) or VWR (UK).

Statistical analysis

The software package IBM SPSS Statistics for Windows (version 19) was used for statistical data evaluation. The Shapiro–Wilk tests were used for data distribution. Most data exhibited a non-normal distribution. Spearman's rank correlation coefficient is normally used when Pearson's correlation coefficient is not valid due to data being clearly non-normal, or where data are provided in the form of ranks rather than in the form of measurements. This coefficient measures the strength of the relationships between PM mass concentration and oxidative activities. The Kruskal–Wallis nonparametric *t* test ($p < 0.05$) was used to test whether the differences between the PM mass concentrations of particulate matter in different particle sizes are statistically significant (Table S4).

Results

PM mass concentrations

Mass concentrations of $PM_{2.5}$, PM_{10}, and TSP samples collected at the ten sites are summarized in Fig. 2 and Table S5. As a result of different activities at the six indoor locations and different spatial locations of the four outdoor sites, PM levels exhibited different mass concentrations. Each type of PM ($PM_{2.5}$, PM_{10}, and TSP) exhibits a variation of more than two orders of magnitude difference. For instance, TSP varies from almost 10^6 (5.6) down to less than 10^3 (2.7), PM_{10} varies between 10^5 (4.7) to 10^3 (2.1), and $PM_{2.5}$ varies from 10^3 (4.0) to 10^2 (1.4). At the ICP site, mass concentrations of TSP (399,245 μg m^{-3}), PM_{10} (45,288 μg m^{-3}), and $PM_{2.5}$ (10,692 μg m^{-3}) exceeded all other sites. Conversely, the outdoor sites (except TB site) away from the mining and processing activities exhibited the lowest values for TSP (<1588 μg m^{-3}), PM_{10} (<332 μg m^{-3}), and $PM_{2.5}$ (<71 μg m^{-3}), together with $PM_{2.5}$ in the HRP (61 μg m^{-3}), where a wet grinding method is used (Table S5).

Morphological, mineralogical, and elemental composition of PM

The results of mineralogical analysis of representative PM and FD samples by XRD (SP_4, SP_5, SP_{10}, SP_{12}, SP_{31}, and SP_{43}) and PLM of thin-polish sections (D_1, D_2, D_4, and D_{10}) are shown in Figs. 3, 4, 5, and Table S6. The major crystalline phases in all samples were calcite, magnetite, tremolite, pyrite, talc, and clay minerals including kaolinite, vermiculite, and illite. Minor components included quartz, dolomite, hematite, actinolite, dioptase, biotite, albite, sphalerite, chalcopyrite, nimite, magnesiohornblende-ferroan, laumontite, diopside, and muscovite. These minerals are inherited from mineralization of iron ore in the region, with details regarding the occurrence and nature of ores and minerals in the deposit discussed in detail elsewhere (Babaki and Aftabi 2006; Mücke and Younessi 1994). This mineralogy is in contrast with that from PM typically found in urban areas, which may change according to PM abundance, type, and grain size, all of which are sensitive to wind direction, seasonal factors, and occurrence of dust events (Ahmady-Birgani et al. 2015). Tremolite and actinolite amphibole asbestos present in PM and rock thin microscopic sections (Fig. 5 and Figure S1).

In several previous mineralogical studies of the GEG area, possible links between actinolitization and iron mineralization (e.g., Asadi and Rajabzadeh 2014; Babaki and Aftabi

2006; Mücke and Younessi 1994; Nabatian et al. 2015), and also presence of tremolite and actinolite in the GEG iron deposit (Fig. S1), have been addressed in detail (Babaki and Aftabi 2006). These minerals can be separated and inhaled during crushing and grinding of iron ores.

According to Rietveld method of calculation based on XRD patterns (Rietveld 1969), the volume percentage of tremolite in iron ore PM reached up to 23.8% of PM_{10} at the PC station and 21.2% of TSP at the TB station (Table S6). Actinolite accounted for 10.3% of TSP at the ICP site and 23.5% of PM_{10} at the PC site. Thus, these asbestos minerals are quite abundant at the study site.

The contribution of crystalline silica (SiO_2) to PM_{10} was estimated to be as high as 7.3% at the PC station. Talc accounted for up to 34.5% of TSP at the ICP station (Table S6). Samples from the PC, R&D Center, and ICP station (samples D_1, D_2, D_{10}, SP_1, SP_5, SP_{10}, SP_{25}) enriched with fibrous-elongated minerals were selected for further SEM/EDS microscopic identification. Tremolite and actinolite were the two key identified constituents using this technique. The morphology and chemical composition of PM, especially needle-shaped minerals, were identified using SEM/EDS (Fig. 6), which confirmed the observations obtained by XRD that the needle-shaped minerals, which are dominated by Ca, Mg, Si, Fe, and Ca, are tremolite and actinolite amphibole asbestos. Although tremolite is a certain phase in the XRD and microscopic studies, EDS chemical analysis results show that the dominant type of amphibole asbestos mineral is actinolite in the GEG dust samples. It is necessary to note that these minerals may occur together and form a continuous mineral series.

According to morphological studies by SEM, the length of needle-shaped minerals in iron ore dust varied between 1.5 nm and 71.65 μm and the diameter ranged between 0.2 nm and 4.26 μm (Figure S2). The results of the elemental distribution in crystal chemistry of actinolite are also given in Table 1. Carbon conductive tabs have been used in SEM mounting so it is presented in EDX graphs.

Oxidative potential of PM samples

Following measurement of the remaining antioxidants left in the 4-h incubated RTLF, data were initially corrected for background oxidation (proved to be less than 5%) and then converted to percentage of antioxidant consumption with reference to the 4-h particle-free (C_4) control. Table S7 and Table 2 show the data of antioxidant consumption and its mean value of the samples (%), grouped by particle size and indoor/outdoor sampling, respectively. $PM_{2.5}$ samples showed higher mean AA consumption during 4 h of incubation as compared to PM_{10} and TSP. Ascorbate consumption for $PM_{2.5}$ was 34.56% for indoor and 32.98% for outdoor samples, respectively (Table 2).

The antioxidant consumption in %OP (Table 2 for mean values and Table S7 for raw data) was converted to oxidative potential per unit of mass of particulate matter (OP μg^{-1} PM) (Table 3 for mean values and Table S8 for raw data) after dividing through by the PM mass used during the RTLF exposure experiment (25 μg or 0.5 mL of a 50 μg mL^{-1} of PM suspension). The OP^{UA} μg^{-1} was calculated to be less than the minimum detection value of

0.2 based on a minimum measurable %OP of 10%. The calculated consumption of UA and GSH per unit of mass is considered null, and hence, these antioxidants will not be reported further. The OP^{AA} μg^{-1} PM is calculated to give an indication of the individual PM toxicity. The iron ore samples displayed lower AA oxidation per unit of mass (OP^{AA} μg^{-1}) as shown in Table 3, ($PM_{2.5}$ = 1.16 and 1.05; PM_{10} = 0.88 and 0.85; and TSP = 1.18 and 0.76 for indoor and outdoor sites, respectively), relative to the London roadside control (OP_{AA} = 2.2 μg^{-1}).

The OP^{AA} μg^{-1} (Table S8) was converted to the ascorbate oxidation per unit of volume (OP^{AA} m^{-3}) (Table S8) by multiplying by the calculated μg PM m^{-3} (Table S8, second column). The data have been broken down into indoor and outdoor and into individual particle sizes and plotted to provide a figure for $PM_{2.5}$, PM_{10}, and TSP based on OP^{AA} m^{-3} (Fig. 7). In this figure, the substantial differences in ascorbate oxidation (OP^{AA} m^{-3}) between sizes and indoor/outdoor PM samples are obvious. The mean OP^{AA} m^{-3} values of PM for indoor places were higher than the outdoor ones. For example, the mean values of OP^{AA} m^{-3} for indoor TSP, $PM_{2.5}$, and PM_{10} were 26.6, 15, and 6 times higher than the outdoor ones, respectively, possibly due to indoor places having a high PM mass concentration. Also, the PM mass concentration in TSP was higher than PM_{10} and $PM_{2.5}$ resulting in higher OP^{AA} m^{-3} values for TSP.

A significant correlation is observed between indoor TSP mass concentration and OP^{AA} m^{-3} (N = 5) (rs = 0.6; p <0.01). However, there is no relationship between outdoor TSP mass concentration and OP^{AA} m^{-3} (N = 5) (rs = −0.4; p <0.01) or between OP^{AA} m^{-3} and either indoor or outdoor $PM_{2.5}$ mass concentration (N = 9) (rs = −0.1; rs = −0.2; p <0.01, respectively), or PM_{10} mass concentration (N = 10) (rs = −0.14; rs = −0.2; p <0.01, respectively).

Discussion

PM mass concentrations

The high PM levels observed in GEG facilities clearly exceed the PM_{10} and the $PM_{2.5}$ values adopted by the US National Ambient Air Quality Standards (NAAQS), 150 and 35 μg m^{-3}, respectively, established by the Environmental Protection Agency (USEPA 2011), as well as the 24-hour mean guideline values established by the World Health Organization (25 μg m^{-3} for $PM_{2.5}$ and 50 μg m^{-3} for PM_{10}) (WHO 2006). This is particularly evident inside the ICP, where three dried production lines operate simultaneously. This strongly suggests that ventilation in GEG facilities is not adequate, leading to great risk for mine workers including vulnerability to respiratory diseases (Petavratzi et al. 2005). Inside the IPP, there are also plenty of fine particles as a result of passing of several crushers, mills, and grinders indicating highly PM exposure at this place for workers. PM mass concentration results showed notably level of PM (Fig. 2). Only two outdoor places (i.e., B No. 45 and R & D Center) exhibit a $PM_{2.5}$ value below the NAAQS limit (Table S5), while the lowest PM_{10} mass concentration is observed near the entrance of the MOO building (113.12 μg m^{-3}), which is below the EPA NAAQ standard. The tailing bin (TB) is classified as an outdoor place in GEG mine, but because of significant PM release during dry ore-processing waste storage and trunk loading of them to waste disposal sites, the mass concentration at this

station showed high values (Fig. 2). The concentration ratio of TSP:$PM_{2.5}$ was 257 at HRP and approximately 100 at the TB and PLY sites (Table S5), highlighting the significant role of mechanical activity (i.e., crushing and grinding) to generate coarse particles, similar to other mines (Csavina et al. 2012).

Morphological, mineralogical, and elemental composition of PM

In the study area, iron ore dusts mainly contain fibrogenic material of a carcinogenic nature, including amphibole asbestos minerals (tremolite and actinolite), silica, mica, and talc. These minerals are some of the most hazardous of the fibrogenic dusts leading to toxic and carcinogenic reactions, and, over long periods of time can produce a fibrous growth of tissue resulting in loss of lung elasticity and greatly reduced area for gas exchange (Meyer et al. 1996). The result is increased stress on the heart and ultimately death due to heart failure (Eby 2004). Inhalation of dust with asbestos fibers can result in lung cancer and mesothelioma of the pleura and peritoneum (Davies and Mundalamo 2010; Shah 2003) in addition to autoimmune diseases (i.e., scleroderma, rheumatoid arthritis) (Noonan et al. 2006; Pfau et al. 2005). Tremolite ($Ca_2(Mg, Fe^{2+})_5(OH, F)_2[Si_8O_{22}]$) and actinolite ($(Ca_2(Mg, Fe^{2+})_5](OH)_2[Si_8O_{22}$) have polymeric structure consists of a linear double chains which crystallize into long, thin, straight fibers, which are the characteristic structure of this type of asbestos (Deer et al. 1992; Veblen and Wylie 1993). They sometimes occur in the form of asbestos, and also in fibrous, radiated, or columnar forms in metamorphic rocks (such as schists) and in altered igneous rocks (Neuendorf 2005). Non-fibrous forms of tremolite, actinolite, and anthophyllite also are found naturally. However, because they are not fibrous, they are not classified as asbestos minerals (US Public Health and Services 2001). Amphibole-group minerals such as actinolite are easily separable when crushed or processed (OSHA 1986).

These minerals form solid solution series (the magnesium-rich tremolite (Fe^{2+}: 0.0–0.5%, Mg: 0.5–4.5%), an intermediate member actinolite (Fe^{2+}: 0.5–2.5%, Mg: 2.5–4.5%), and an iron-rich ferroactinolite (Fe^{2+}: 2.5–5.0%, Mg: 0–2.5%) series) (Klein et al. 1993, 2002), since they show a range of chemical formulas as a result of ion or ionic group substitutions. Tremolite and actinolite form such a continuous mineral series in which Mg and Fe(II) can freely substitute with each other while retaining the same three-dimensional crystal structure (Monoclinic) (US Public Health and Services 2001; Veblen and Wylie 1993). Tremolite has little or no iron while actinolite contains iron and may contain manganese (Jolicoeur et al. 1992; Ross and Virta 2001; Skinner et al. 1988).

The definition of how much Fe must be present before tremolite becomes actinolite is not universally recognized and has changed over time (Wylie and Verkouteren 2000). Wylie and Verkouteren (2000) also cited the amphiboles which form a solid solution series and are not regulated under Federal Regulations (EPA 1987; OSHA 1998).

For regulatory purposes, these minerals are considered to be fibrous if they have a length of greater than 5 μm, a diameter of less than 5 μm, and aspect ratio (length to width or diameter) of 3:1 or greater. The mineralogical community uses a greater aspect ratio of 10:1 or 20:1 to define fibrous minerals (Eby 2004). In this study, SEM results indicate that the range of the length-to-diameter ratio of all fibrous minerals is between 7.5 and 24, so they

can be considered as asbestiform fibrous minerals which pose a significant health risk to the exposed workers. Nevertheless, in examined samples SP_{12} and D_5 by SEM, which were taken from IPP, no specified fiber minerals was observed due to removing of waste minerals and purification during iron ore processing.

Additional fibrogenic minerals in iron dust include silica (SiO_2) and talc ($Mg_3Si_4O_{10}(OH)_2$. Individuals exposed to fibrogenic mineral dust may exhibit an impaired antioxidant system and produce high levels of reactive oxygen and nitrogen species through immune cells, contributing to the perturbation of immune cell function, inflammation, fibrosis, and lung cancer (Muzembo et al. 2015). Previous studies have reported that diseases such as silicosis, tuberculosis, scleroderma, and rheumatoid arthritis may originate from exposure to silica (Ehrlich et al. 2006; Gibbons 2000; Mannetje et al. 2002; Noonan et al. 2006). Banerjee et al. (2006) reported that silica is a probable contributor to the elevated incidence of lung cancer among iron ore dust-exposed workers. Talc has been shown to cause talcosis and talc pneumoconiosis in workers exposed to high levels during mining and processing operations (Banks and Parker 1998). These studies have illustrated that long-term exposure and inhalation of particles containing fibrogenic minerals such as asbestos, talc and crystalline silica can increase the potential risk on human health.

Oxidative potential of PM samples

Among the three low molecular weight antioxidants of the synthetic RTLF, the samples mainly displayed a reactivity only with the ascorbate, and a negligible amount of oxidation with both the GSH and urate. The absence of an impact of PM exposure on UA defenses indicates both that the oxidant component of PM is not at a toxic level in this study and that an important component of the RTLF antioxidant network appears ineffective against the active components of PM. This was supported by the failure of any of the particle types to deplete UA from the synthetic RTLF model (Mudway et al. 2004).

Past experience with a variety of PM samples has shown that despite the fact that UA is a highly effective hydroxyl radical scavenger (Kaur and Halliwell 1990), the urate is not usually susceptible to oxidation by PM (Künzli et al. 2006; Szigeti et al. 2014).

Szigeti et al. (2014) observed that among the three low molecular weight antioxidants of the synthetic RTLF, only AA and GSH were oxidized and urate was shown to be inert to $PM_{2.5}$ samples in five office buildings in Hungary. Mudway et al. (2004) reported that filter extracts of diesel engine (DE) particulate emissions, placed in the sham exposure chamber, depleted lung lining fluid antioxidants AA and GSH but not UA. Zielinski et al. (1999) found a significant difference in the overall depletion rates between GSH, AA, and UA, suggesting an overall reactivity hierarchy within the pure antioxidant model (individual antioxidant solutions) of GSH > AA $\gg$ UA. They also demonstrated that the depletion kinetics seen for each antioxidant was quite different (Zielinski et al. 1999). Our results support the statement that different respiratory pollutants may target different antioxidants.

The rate of depletion of the different antioxidants is largely dependent on the PM chemical composition (Künzli et al. 2006; Mudway et al. 2004; Zielinski et al. 1999). For example, GSH has shown a higher sensitivity to Cu-catalyzed oxidation (Ayres et al. 2008). Szigeti et

al. (2014) found a significant correlation between OP^{GSH} μg^{-1} and Cr and Zn concentration for the $PM_{2.5}$ samples in five office buildings in Hungary. In the present study, GSH is not depleted by PM samples. The low content of these certain metals might be the cause.

The depletion of AA related to the $PM_{2.5,}$ PM_{10}, and TSP mass was always higher in the case of indoor samples. Taking into account all samples, the TSP samples related to indoor and outdoor OP values were higher than the corresponding $PM_{2.5}$ and PM_{10} in the case of AA (Fig. 7). Following the same pattern, the mass concentration was higher in the indoor samples, and also in the TSP samples. Therefore, our OP^{AA} m^{-3} results reveal the important effect of mass concentration on antioxidant oxidation. However, the appreciable correlation only between indoor TSP mass concentration and OP^{AA} m^{-3} indicates that PM mass concentration alone is not responsible for PM oxidative activity, and other factors such as PM size or chemical composition might also affect it. Godri et al. (2010b) found that high PM_{10} mass concentrations coinciding with elevated transition metal levels lead to high oxidative potential. Likewise, Janssen et al. (2014) and Delfino et al. (2013) observed a high correlation between the consumption of dithiothreitol ($OP^{DTT\text{-}PM}$ $_{2.5}$) (expressed per m^3) and PM mass concentration. Szigeti et al. (2014) found that PM chemical composition is more important than PM mass concentration with regard to oxidative potential of $PM_{2.5}$ samples. The levels of AA oxidation per unit of volume (OP^{AA} m^{-3}) found in this study were extremely high. For example, levels of OP^{AA} m^{-3} for outdoor $PM_{2.5}$, PM_{10}, and TSP were 60, 580, and 2846 orders of magnitude higher, respectively, than LDN (Table 3).

This metric is a suitable indicator of the toxicity of the surrounding working environment. The observations (based on the combination of supplied total PM mass on the filter and total m^3 volume) indicate that very high levels of PM are present in the surrounding environment and this results in very high OP^{AA} m^{-3} in comparison with that which would normally be observed at London roadsides (average ± SD: 5.32 ± 4.52) (Godri et al. 2011).

Conclusion

This study examined mass concentration, mineralogy, and oxidative potential (OP) of iron ore particulate matter in TSP, PM_{10}, and $PM_{2.5}$ at the Gol-E-Gohar Mining and Industrial Facility in southern Iran. Results of mineralogical studies revealed that some hazardous minerals such as tremolite, actinolite, crystalline silica, and talc were present in samples collected at various sites around the study area. The small sizes of PM containing theses minerals can be inhaled during direct exposure to particulate matter. The mass concentration of iron ore is higher inside the ore processing plants compared to outdoor sites nearby the entrance of office buildings.

The iron ore samples were found to have oxidative activity but only against the antioxidant, ascorbic acid. No substantial activity was observed against uric acid or reduced glutathione (GSH). Although the oxidant activity against ascorbic acid was low to medium per unit of mass in relation to the other sources of PM (i.e., urban road side), the high mass concentration of iron ore found at the facility indicates that workers in this environment are exposed to a considerable oxidative load from inhaled PM.

The results motivate implementation of basic control strategies to reduce the mass concentration of particulate matter and to help improve air quality including the use of PM protection equipment by exposed persons, and application of ventilation and air cleaner systems inside the facility. The duration and magnitude of exposure to dust for mine workers who suffer from lung diseases should be limited via worker rotation and job task changes.

Iron ore mining and processing at the GEG complex started in recent years (~20 years), and thus, records may be limited for worker exposure (except a few cases) because the inhaled minerals may have a long latency period. Exposed workers need to be examined periodically for some regular respiratory tests (e.g., chest C.T scan and spirometry test) in order to determine early symptoms. Routine environmental monitoring, epidemiological studies, and chemical composition evaluation of iron ore dust are also recommended.

Supplementary Material

Refer to Web version on PubMed Central for supplementary material.

Acknowledgments

This work was financially supported by Gol-E-Gohar mining and industrial company. The authors wish to thank Shiraz University Research Committee and medical geology research center of Shiraz University for supporting this research. AS acknowledges support from Grant 2 P42 ES04940 from the National Institute of Environmental Health Sciences (NIEHS) Superfund Research Program, NIH and the Center for Environmentally Sustainable Mining through the TRIF Water Sustainability Program at the University of Arizona. The University Spectroscopy and Imaging Facility (USIF) at the University of Arizona is acknowledged for assistance with SEM/EDX analysis.

References

Ahmady-Birgani H, Mirnejad H, Feiznia S, McQueen KG. Mineralogy and geochemistry of atmospheric particulates in western Iran. Atmospheric Environment. 2015; 119:262–272.

Alavi M. Regional stratigraphy of the Zagros fold-thrust belt of Iran and its proforeland evolution. American Journal of Science. 2004; 304(1):1–20.

Amato F, Pandolfi M, Viana M, Querol X, Alastuey A, Moreno T. Spatial and chemical patterns of PM 10 in road dust deposited in urban environment. Atmospheric Environment. 2009; 43(9):1650–1659.

Asadi S, Rajabzadeh MA. Geochemistry, paragenesis, and wall-rock alteration of the qatruyeh iron deposits, southwest of Iran: Implications for a hydrothermal-metasomatic genetic model. Journal of Geological Research. 2014; 2014:590540.doi: 10.1155/2014/590540

Ayres JG, Borm P, Cassee FR, Castranova V, Donaldson K, Ghio A, et al. Evaluating the toxicity of airborne particulate matter and nanoparticles by measuring oxidative stress potential—A workshop report and consensus statement. Inhalation Toxicology. 2008; 20(1):75–99. [PubMed: 18236225]

Azadeh A, Osanloo M, Ataei M. A new approach to mining method selection based on modifying the Nicholas technique. Applied Soft Computing. 2010; 10(4):1040–1061.

Babaki A, Aftabi AJ. Investigation on the model of iron mineralization at Gol Gohar iron deposit, Sirjan-Kerman. Geosciences Scientific Quarterly Journal. 2006; 61:40–59.

Baker MA, Cerniglia GJ, Zaman A. Microtiter plate assay for the measurement of glutathione and glutathione disulfide in large numbers of biological samples. Analytical Biochemistry. 1990; 190(2): 360–365. [PubMed: 2291479]

Banerjee KK, Wang H, Pisaniello D. Iron-ore dust and its health impacts. Environmental Health. 2006; 6(1):11.

Banks DE, Parker JE. Occupational lung disease: An international perspective. London: Chapman & Hall Medical; 1998.

Berndt ME, Brice WC. The origins of public concern with taconite and human health: Reserve Mining and the asbestos case. Regulatory Toxicology and Pharmacology. 2008; 52(1):S31–S39. [PubMed: 18055081]

Bhattacharjee P, Paul S. Risk of occupational exposure to asbestos, silicon and arsenic on pulmonary disorders: Understanding the genetic-epigenetic interplay and future prospects. Environmental Research. 2016; 147:425–434. [PubMed: 26966890]

Bish DL. Quantitative X-ray diffraction analysis of soils. Quantitative methods in soil mineralogy, (quantitativemet). 1994:267–295.

Bish DL, Post JE. Quantitative mineralogical analysis using the Rietveld full-pattern fitting method. The American Mineralogist. 1993; 78(9–10):932–940.

Borm PJA, Kelly F, Künzli N, Schins RPF, Donaldson K. Oxidant generation by particulate matter: From biologically effective dose to a promising, novel metric. Occupational and Environmental Medicine. 2007; 64(2):73–74. [PubMed: 17272658]

Boyd JT, Doll R, Faulds JS, Leiper J. Cancer of the lung in iron ore (haematite) miners. British Journal of Industrial Medicine. 1970; 27(2):97–105. [PubMed: 5448525]

Brunner WM, Williams AN, Bender AP. Investigation of exposures to commercial asbestos in northeastern Minnesota iron miners who developed mesothelioma. Regulatory Toxicology and Pharmacology. 2008; 52(1):S116–S120. [PubMed: 17988773]

Chakraborty MK, Ahmad M, Singh RS, Pal D, Bandopadhyay C, Chaulya SK. Determination of the emission rate from various opencast mining operations. Environmental Modelling and Software. 2002; 17(5):467–480.

Chau N, Benamghar L, Pham QT, Teculescu D, Rebstock E, Mur JM. Mortality of iron miners in Lorraine (France): Relations between lung function and respiratory symptoms and subsequent mortality. British Journal of Industrial Medicine. 1993; 50(11):1017–1031. [PubMed: 8280627]

Chen SY, Hayes RB, Liang SR, Li QG, Stewart PA, Blair A. Mortality experience of haematite mine workers in China. British Journal of Industrial Medicine. 1990; 47(3):175–181. [PubMed: 2328225]

Chipera SJ, Bish DL. Fitting full X-ray diffraction patterns for quantitative analysis: A method for readily quantifying crystalline and disordered phases. Advances in Materials Physics and Chemistry. 2013; 3(1A):30340.doi: 10.4236/ampc.2013.31A007

Chuang HC, BéruBé K, Lung SCC, Bai KJ, Jones T. Investigation into the oxidative potential generated by the formation of particulate matter from incense combustion. Journal of Hazardous Materials. 2013; 244:142–150. [PubMed: 23246950]

Clemente R, Paredes C, Bernal MP. A field experiment investigating the effects of olive husk and cow manure on heavy metal availability in a contaminated calcareous soil from Murcia (Spain). Agriculture, Ecosystems & Environment. 2007; 118(1):319–326.

Csavina J, Field J, Taylor MP, Gao S, Landázuri A, Betterton EA, et al. A review on the importance of metals and metalloids in atmospheric dust and aerosol from mining operations. Science of the Total Environment. 2012; 433:58–73. [PubMed: 22766428]

Davies TC, Mundalamo HR. Environmental health impacts of dispersed mineralisation in South Africa. Journal of African Earth Sciences. 2010; 58(4):652–666.

Deer WA, Howie RA, Zussman J. An introduction to the rock-forming minerals. Vol. 696. London: Longman; 1992.

Delfino RJ, Staimer N, Tjoa T, Gillen DL, Schauer JJ, Shafer MM. Airway inflammation and oxidative potential of air pollutant particles in a pediatric asthma panel. Journal of Exposure Science & Environmental Epidemiology. 2013; 23(5):466–473. [PubMed: 23673461]

Dellinger B, Pryor WA, Cueto R, Squadrito GL, Hegde V, Deutsch WA. Role of free radicals in the toxicity of airborne fine particulate matter. Chemical Research in Toxicology. 2001; 14(10):1371–1377. [PubMed: 11599928]

Eberl DD. User guide to RockJock-A program for determining quantitative mineralogy from X-ray diffraction data. US Geological Survey; 2003.

Eby GN. Principles of environmental geochemistry. USA: Brooks/Cole Publishing Company; 2004.

Ehrlich RI, Churchyard GJ, Pemba L, Dekker K, Vermeis M, White NW, et al. Tuberculosis and silica exposure in South African gold miners. Occupational and Environmental Medicine. 2006; 63(3): 187–192. [PubMed: 16497860]

EPA. Asbestos-containing materials in schools. U.S. Environmental Protection Agency; 1987. Federal Register 40CFR 763

EPA. National ambient air quality standards for particulate matter; Final rule. Environmental Protection Agency; 2006. Part II, 40 CFR Part 50

Fantel AG. Reactive oxygen species in developmental toxicity: Review and hypothesis. Teratology. 1996; 53(3):196–217. [PubMed: 8761887]

Gibbons W. Amphibole asbestos in Africa and Australia: Geology, health hazard and mining legacy. Journal of the Geological Society. 2000; 157(4):851–858.

Godri KJ, Duggan ST, Fuller GW, Baker T, Green D, Kelly FJ, et al. Particulate matter oxidative potential from waste transfer station activity. Environmental Health Perspectives. 2010a; 118(4): 493. [PubMed: 20368130]

Godri KJ, Green DC, Fuller GW, Dall'sOsto M, Beddows DC, Kelly FJ, et al. Particulate oxidative burden associated with firework activity. Environmental Science and Technology. 2010b; 44(21): 8295–8301. [PubMed: 20886897]

Godri KJ, Harrison RM, Evans T, Baker T, Dunster C, Mudway IS, et al. Increased oxidative burden associated with traffic component of ambient particulate matter at roadside and urban background schools sites in London. PLoS ONE. 2011; 6(7):e21961. [PubMed: 21818283]

Hendryx M. Mortality from heart, respiratory, and kidney disease in coal mining areas of Appalachia. International Archives of Occupational and Environmental Health. 2009; 82(2):243–249. [PubMed: 18461350]

Heydari E. Tectonics versus eustatic control on super-sequences of the Zagros Mountains of Iran. Tectonophysics. 2008; 451(1):56–70.

Hosseini SA, Asghari O. Multivariate geostatistical simulation of the Gole Gohar iron ore deposit, Iran. Journal of the Southern African Institute of Mining and Metallurgy. 2016; 116(5):423–430.

Iriyama K, Yoshiura M, Iwamoto T, Ozaki Y. Simultaneous determination of uric and ascorbic acids in human serum by reversed-phase high-performance liquid chromatography with electrochemical detection. Analytical Biochemistry. 1984; 141(1):238–243. [PubMed: 6496931]

Jahanshahi R, Zare M. Assessment of heavy metals pollution in groundwater of Golgohar iron ore mine area, Iran. Environmental Earth Sciences. 2015; 74(1):505–520.

Janssen NAH, Yang A, Strak M, Steenhof M, Hellack B, Gerlofs-Nijland ME, et al. Oxidative potential of particulate matter collected at sites with different source characteristics. Science of the Total Environment. 2014; 472:572–581. [PubMed: 24317165]

Jolicoeur CR, Alary J, Sokov A. Asbestos. Kirk-Othmer Encyclopedia of Chemical Technology. 1992; doi: 10.1002/0471238961.0119020510151209.a01

Kamp DW, Weitzman SA. The molecular basis of asbestos induced lung injury. Thorax. 1999; 54(7): 638–652. [PubMed: 10377212]

Kaur H, Halliwell B. Action of biologically-relevant oxidizing species upon uric acid. Identification of uric acid oxidation products. Chemico-Biological Interactions. 1990; 73(2–3):235–247. [PubMed: 2155712]

Kelly F, Anderson HR, Armstrong B, Atkinson R, Barratt B, Beevers S, et al. The impact of the congestion charging scheme on air quality in London. Part 1. Emissions modeling and analysis of air pollution measurements. Research Report (Health Effects Institute). 2011; 155:5–71.

Kinlen LJ, Willows AN. Decline in the lung cancer hazard: A prospective study of the mortality of iron ore miners in Cumbria. British Journal of Industrial Medicine. 1988; 45(4):219–224. [PubMed: 3377997]

Klein C, Hurlbut CS, Dana JD. Manual of mineralogy. New York: Wiley; 1993.

Klein C, Hurlbut CS, Dana JD. The 22nd edition of the manual of mineral science:(after James D. Dana). 2002.

Künzli N, Mudway IS, Götschi T, Shi T, Kelly FJ, Cook S, et al. Comparison of oxidative properties, light absorbance, and total and elemental mass concentration of ambient PM 2.5 collected at 20 European sites. Environmental health perspectives. 2006; 114(5):684–690. [PubMed: 16675421]

Lal B, Tripathy SS. Prediction of dust concentration in open cast coal mine using artificial neural network. Atmospheric Pollution Research. 2012; 3(2):211–218.

Li N, Sioutas C, Cho A, Schmitz D, Misra C, Sempf J, et al. Ultrafine particulate pollutants induce oxidative stress and mitochondrial damage. Environmental Health Perspectives. 2003; 111(4):455. [PubMed: 12676598]

Liu G, Cheresh P, Kamp DW. Molecular basis of asbestos-induced lung disease. Annual Review of Pathology. 2013; 8:161.

Love RG, Miller BG, Groat SK, Hagen S, Cowie HA, Johnston PP, et al. Respiratory health effects of opencast coalmining: A cross sectional study of current workers. Occupational and Environmental Medicine. 1997; 54(6):416–423. [PubMed: 9245948]

Mannetje A, Steenland K, Attfield M, Boffetta P, Checkoway H, DeKlerk N, et al. Exposure-response analysis and risk assessment for silica and silicosis mortality in a pooled analysis of six cohorts. Occupational and Environmental Medicine. 2002; 59(11):723–728. [PubMed: 12409529]

Meyer C, Du Plessis JJL, Oberholzer JW. Handbook to reduce the exposure of workers to dust. Safety in Mines Research Advisory Committee. 1996:1–157. COL 027.

Mirnejad H, Simonetti A, Molasalehi F. Pb isotopic compositions of some Zn–Pb deposits and occurrences from Urumieh–Dokhtar and Sanandaj–Sirjan zones in Iran. Ore Geology Reviews. 2011; 39(4):181–187.

Monjezi M, Shahriar K, Dehghani H, Samimi Namin F. Environmental impact assessment of open pit mining in Iran. Environmental Geology. 2009; 58:205–216.

Mücke A, Golestaneh F. The genesis of the Gol Gohar iron ore deposit (Iran). Institu fur Mineralogie und Kritallographieder Technischen Universitat Berlin. 1982; 41:193–212.

Mücke A, Younessi R. Magnetite-apatite deposits (Kiruna-type) along the Sanandaj-Sirjan zone and in the Bafq area, Iran, associated with ultramafic and calcalkaline rocks and carbonatites. Mineralogy and Petrology. 1994; 50(4):219–244.

Mudway IS, Stenfors N, Duggan ST, Roxborough H, Zielinski H, Marklund SL, et al. An in vitro and in vivo investigation of the effects of diesel exhaust on human airway lining fluid antioxidants. Archives of Biochemistry and Biophysics. 2004; 423(1):200–212. [PubMed: 14871482]

Muzembo BA, Deguchi Y, Ngatu NR, Eitoku M, Hirota R, Suganuma N. Selenium and exposure to fibrogenic mineral dust: A mini-review. Environment International. 2015; 77:16–24. [PubMed: 25615721]

Nabatian G, Rastad E, Neubauer F, Honarmand M, Ghaderi M. Iron and Fe–Mn mineralisation in Iran: Implications for Tethyan metallogeny. Australian Journal of Earth Sciences. 2015; 62(2):211–241.

Nel A. Air pollution-related illness: Effects of particles. Science. 2005; 308(5723):804–806. [PubMed: 15879201]

Neuendorf KKE. Glossary of geology. New York: Springer Science & Business Media; 2005.

Noonan CW, Pfau JC, Larson TC, Spence MR. Nested case-control study of autoimmune disease in an asbestos-exposed population. Environmental health perspectives. 2006; 114(8):1243–1247. [PubMed: 16882533]

OSHA. Occupational Exposure to Asbestos, Tremolite, Anthophyllite, and Actinolite: Final Rules. Federal Register. 1986; 51

OSHA. Occupational Safety and Health Administration. Code of Federal Regulations. 1998 29 CFR 1910.1001.

Park SS, Wexler AS. Size-dependent deposition of particles in the human lung at steady-state breathing. Journal of Aerosol Science. 2008; 39(3):266–276.

Patra AK, Gautam S, Kumar P. Emissions and human health impact of particulate matter from surface mining operation—A review. Environmental Technology & Innovation. 2016; 5:233–249.

Petavratzi E, Kingman S, Lowndes I. Particulates from mining operations: A review of sources, effects and regulations. Minerals Engineering. 2005; 18(12):1183–1199.

Pfau JC, Sentissi JJ, Weller G, Putnam EA. Assessment of autoimmune responses associated with asbestos exposure in Libby, Montana, USA. Environmental Health Perspectives. 2005; 113(1):25–30. [PubMed: 15626643]

Phillips J. The application of a mathematical model of sustainability to the results of a semi-quantitative environmental impact assessment of two iron ore opencast mines in Iran. Applied Mathematical Modelling. 2013; 37(14):7839–7854.

Plumlee GS, Morman SA, Ziegler TL. The toxicological geochemistry of earth materials: An overview of processes and the interdisciplinary methods used to understand them. Reviews in Mineralogy and Geochemistry. 2006; 64(1):5–57.

Rietveld H. A profile refinement method for nuclear and magnetic structures. Journal of Applied Crystallography. 1969; 2(2):65–71.

Ross M, Nolan RP, Nord GL. The search for asbestos within the Peter Mitchell Taconite iron ore mine, near Babbitt, Minnesota. Regulatory Toxicology and Pharmacology. 2008; 52(1):S43–S50. [PubMed: 18060674]

Ross M, Virta RL. Occurrence, production and uses of asbestos. Canadian Mineralogist Special Publications. 2001; 5:79–88.

Saadat M, Khandelwal M, Monjezi M. An ANN-based approach to predict blast-induced ground vibration of Gol-E-Gohar iron ore mine, Iran. Journal of Rock Mechanics and Geotechnical Engineering. 2014; 6(1):67–76. DOI: 10.1016/j.jrmge.2013.11.001

Sabzehei M, Eshraghi SA, Roshan Ravan J, Seraj M. Geological map of Gole Gohar area, scale 1:100,000. 1997

Saeidi O, Torabi SR, Ataei M, Rostami J. A stochastic penetration rate model for rotary drilling in surface mines. International Journal of Rock Mechanics and Mining Sciences. 2014; 68:55–65.

Sahai N, Schoonen MAA, Skinner HCW. The emergent field of medical mineralogy and geochemistry. Reviews in Mineralogy and Geochemistry. 2006; 64(1):1–4.

Shah CP. Public health and preventive medicine in Canada. WB Saunders Company Canada Limited; 2003.

Shi T, Knaapen AM, Begerow J, Birmili W, Borm PJA, Schins RPF. Temporal variation of hydroxyl radical generation and 8-hydroxy-2′-deoxyguanosine formation by coarse and fine particulate matter. Occupational and Environmental Medicine. 2003; 60(5):315–321. [PubMed: 12709515]

Singh G, Pal A, Khoiyanbam RS. Impact of mining on human health in and around Jhansi, Bundelkhand region of Uttar Pradesh, India. Journal of Ecophysiology and Occupational Health. 2009; 9(1/2):47.

Sinha S, Banerjee SP. Characterization of haul road dust in an Indian opencast iron ore mine. Atmospheric Environment. 1997; 31(17):2809–2814.

Skinner HCW, Ross M, Frondel C. Asbestos and other fibrous materials: Mineralogy, crystal chemistry, and health effects. Oxford: Oxford University Press; 1988.

Stafilov T, Šajn R, Pančevski Z, Boev B, Frontasyeva MV, Strelkova LP. Heavy metal contamination of topsoils around a lead and zinc smelter in the Republic of Macedonia. Journal of Hazardous Materials. 2010; 175(1):896–914. [PubMed: 19944530]

Szigeti T, Kertész Z, Dunster C, Kelly FJ, Záray G, Mihucz VG. Exposure to PM 2.5 in modern office buildings through elemental characterization and oxidative potential. Atmospheric Environment. 2014; 94:44–52.

US Public Health, & Services, U. S. D. of H. and H. Toxicological profile for asbestos. Atlanta, GA: Agency for Toxic Substances and Disease Registry; 2001.

USEPA. Speciation Guidance (Final Draft). US Environmental Protection Agency; Research Triangle Park, NC: 1999.

USEPA. National Ambient Air Quality Standards (NAAQS). US Environmental Protection Agency; Research Triangle Park, NC. Washington, D.C: 2011.

Valko M, Morris H, Cronin MTD. Metals, toxicity and oxidative stress. Current Medicinal Chemistry. 2005; 12(10):1161–1208. [PubMed: 15892631]

Veblen DR, Wylie AG. Mineralogy of amphiboles and 1: 1 layer silicates. Washington, DC (United States): Mineralogical Society of America; 1993.

WHO. Air quality guidelines: Global update 2005: Particulate matter, ozone, nitrogen dioxide, and sulfur dioxide. World Health Organization; 2006.

Wild P, Bourgkard E, Paris C. Lung cancer and exposure to metals: The epidemiological evidence. Cancer Epidemiology: Modifiable Factors. 2009; 472:139–167.

Williams PJ, Barton MD, Johnson DA, Fontboté L, De Haller A, Mark G, et al. Iron oxide copper-gold deposits: Geology, space-time distribution, and possible modes of origin. Economic Geology. 2005; 100th Anniversary Volume:371–405.

Wylie AG, Verkouteren JR. Amphibole asbestos from Libby, Montana: Aspects of nomenclature. American Mineralogist. 2000; 85(10):1540–1542.

Zielinski H, Mudway IS, Bérubé KA, Murphy S, Richards R, Kelly FJ. Modeling the interactions of particulates with epithelial lining fluid antioxidants. American Journal of Physiology-Lung Cellular and Molecular Physiology. 1999; 277(4):L719–L726.

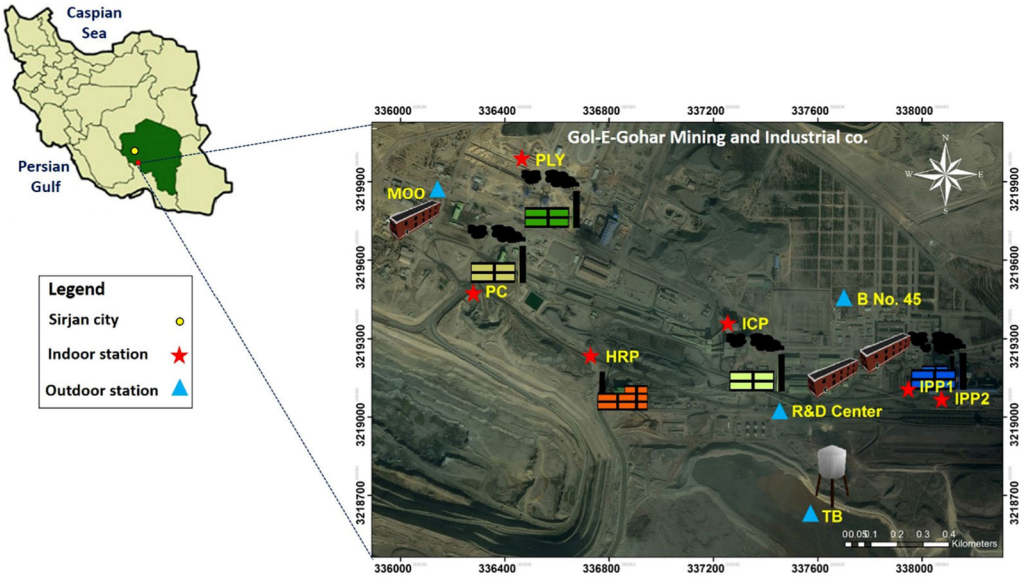

Fig. 1.

Sampling locations for PM and fallout dust samples around the GEG facilities. Indoor areas including the following ($N = 6$): iron ore processing plants (i.e., IPP_1 before furnace and IPP_2 after furnace), iron ore concentration plant (ICP), hematite recovery plant (HRP), primary crusher (PC), and polycom plant (PLY). Outdoor areas included the following ($N = 4$): tail bin (TB), building number 45 (B No. 45; an official building), the Research and Development Center (R&D Center), and the Mining Operation Office (MOO)

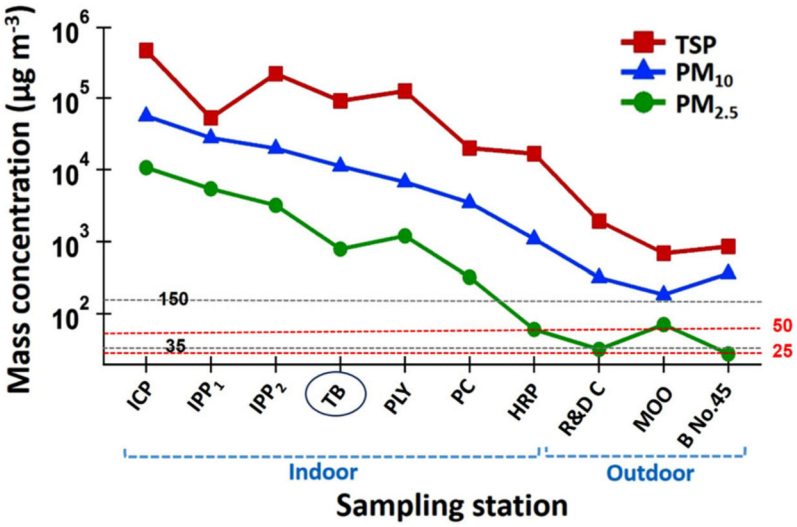

Fig. 2.

Mean mass concentrations of $PM_{2.5}$, PM_{10}, and TSP at the ten sites in the GEG mine over the study period duration (December 17 2014–May 21 2015). Two *horizontal lines* are added representing the US NAAQS limits for $PM_{2.5}$ (35 µg m^{-3}) and PM_{10} (150 µg m^{-3}) and two *red lines* show WHO 24-h standards for $PM_{2.5}$ (25 µg m^{-3}) and for PM_{10} (50 µg m^{-3}). The indoor and outdoor stations were divided except for the TB station, which was grouped with indoor stations owing to its high concentrations

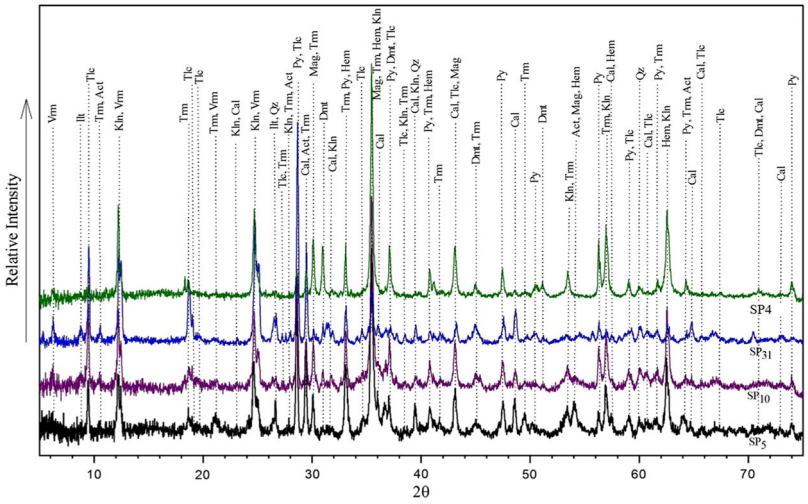

Fig. 3.

X-ray diffraction patterns for bulk mineral composition obtained from PM samples (Abbreviations, *Hem* hematite, *Qz* quartz, *Mag* magnetite, *Tlc* talc, *Kln* kaolinite, *Atc* actinolite, *Cal* calcite, *Trm* tremolite, *Vrm* vermiculite, *Ilt* illite, *Py* pyrite, and *Dol* dolomite). The goodness of fit (GOF) indicator was: $X^2 = 2.56$ for SP_5 (the *black graph*), $X^2 = 2.74$ for SP_{10} (the *purple graph*), $X^2 = 2.28$ for SP_{31} (the *blue graph*), and $X^2 = 2.56$ for SP_4 (the *green graph*)

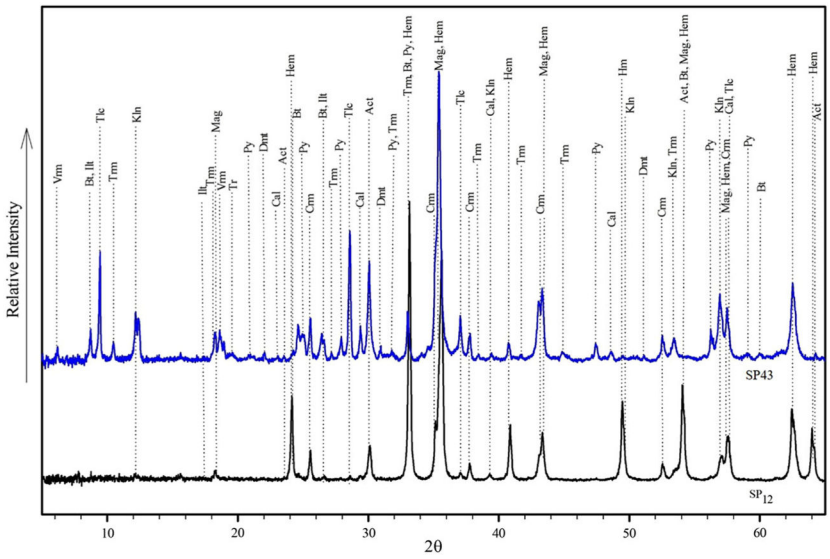

Fig. 4.

X-ray diffraction patterns for QXRD analysis of PM samples (SP_{12} and SP_{43}) run with 20% Corundum (Abbreviation, *Hm* hematite, *Crn* corundum, *Mag* magnetite, *Bt* biotite, *Tlc* talc, *Kln* kaolinite, *Act* actinolite, *Cal* calcite, *Trm* tremolite, *Vrm* vermiculite, *Ilt* illite, *Py* pyrite, *Dol* dolomite). The goodness of fit (GOF) indicator was: $X^2 = 1.63$ for SP_{12} (the *black graph*) and $X^2 = 1.56$ for SP_{43} (the *blue graph*)

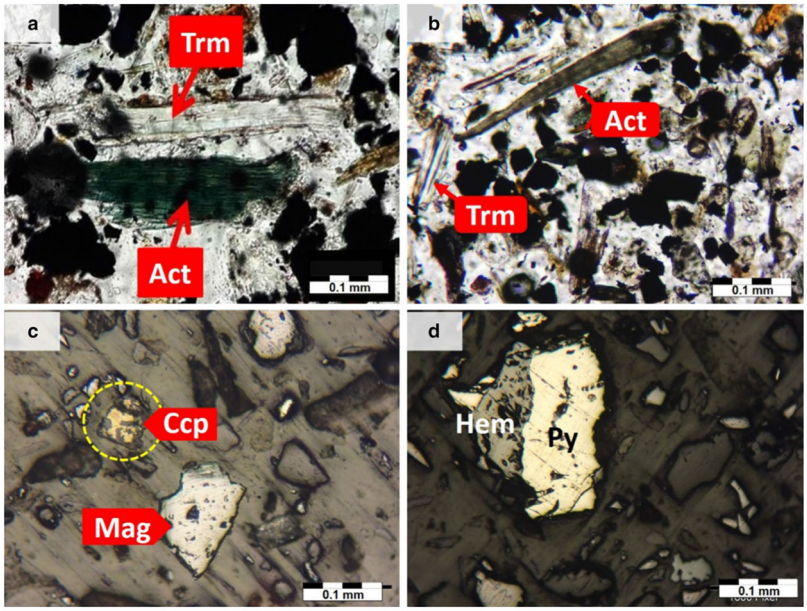

Fig. 5.

Thin-polish section photomicrographs of the various minerals and ores in fallout dust: **a** actinolite (Act) and tremolite (Trm) in sample D_1 (PPL, scale 0.1 mm); **b** tremolite and actinolite in sample D_2 (PPL, 0.1 mm); **c** magnetite (Mag) and chalcopyrite in sample D_{10} (Ccp) (RL, 0.1 mm); **d** pyrite (P) and hematite in sample D_4 (Hem) (RL, 0.1 mm). *PPL* plane polarized light; *RL* reflected light

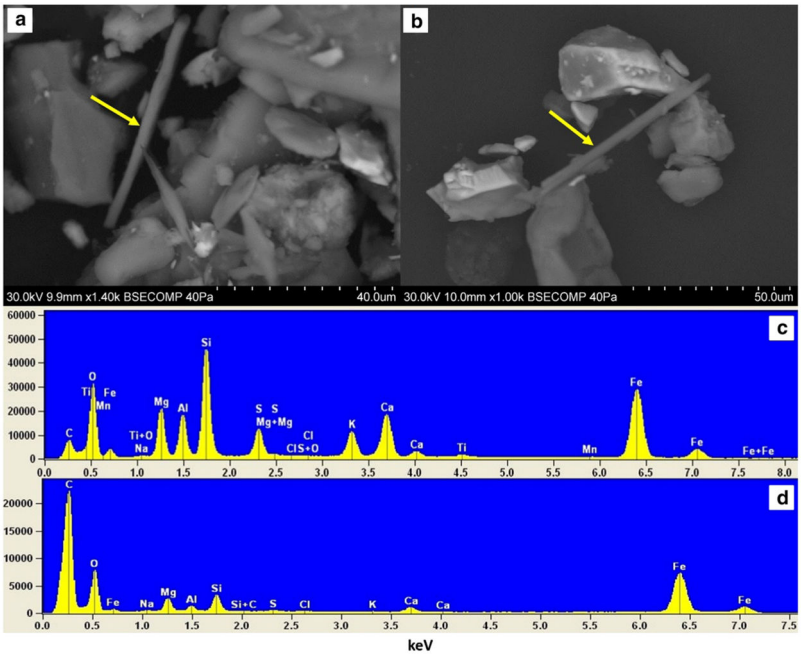

Fig. 6.

Scanning electron microscope (SEM) of PM and fallout dust: **a** images of fibrous-elongated minerals in sample D_{10} including the marked actinolite that is 67.61 μm in length and 3.10 μm in diameter and the smaller one with 36.74 μm in length and 4.26 μm in diameter with a sharp side of 1.87 μm in diameter; **b** needle-shaped actinolite in sample SP_5, 71.05 μm in length and 3.47 μm in diameter; **c**, **d** energy-dispersive spectrum showing elemental composition of the *marked area* in **a** and **b**

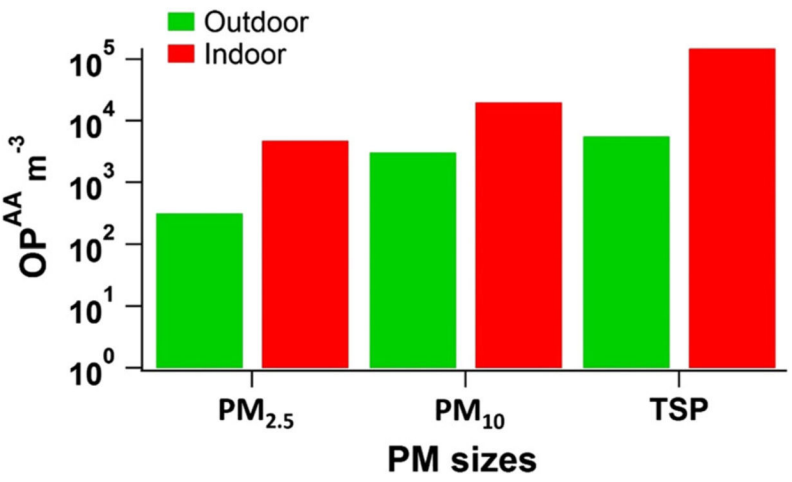

Fig. 7.

Indoor and outdoor OP^{AA} m^{-3} data for $PM_{2.5}$, PM_{10}, and TSP. Abbreviations: OP^{AA} m^{-3}, AA depletion per unit volume

Table 1

Diameter, length, and elemental distribution (% atoms) of actinolite fibers for five different samples (L/D ratio: length to diameter ratio, Std D: standard deviation)

Sample	Length (μm)	Diameter (μm)	L/D ratio	O (at%)	Na (at%)	Mg (at%)	Al (at%)	Si (at%)	S (at%)	Cl (at%)	K (at%)	Ca (at%)	Ti (at%)	Mn (at%)	Fe s(at%)
D_1	67.61	3.10	21.81	40.75	0.11	3.36	2.15	4.92	1.11	0.03	0.76	1.46	0.09	0.03	3.51
SP_6	36.74	2.26	16.26	22.74	0.06	0.67	0.18	0.5	0.03	0.02	0.01	0.14	ND	ND	1.74
D_3	71.05	3.47	20.48	42.44	ND	3.94	1.89	4.76	0.15	0.07	0.65	0.8	0.08	0.02	3.25
D_4	55.46	3.65	15.19	22.58	0.04	1.67	0.16	2.46	0.21	0.01	0.01	0.13	ND	ND	2.47
D_{10}	7.35	0.41	17.93	24.2	0.04	1.05	0.16	1.01	0.05	0.01	0.01	0.12	ND	ND	1.87
SP_2	0.38	0.02	24.24	33.66	ND	3.36	0.07	4.62	0.21	0.01	ND	0.06	ND	ND	1.25
SP_5	0.0015	0.0002	7.50	28.71	0.05	1.93	0.15	2.41	ND	0.01	0.01	0.09	ND	ND	1.53
Mean	34.08	1.84	18.52	30.73	0.06	2.28	0.68	2.95	0.29	0.02	0.24	0.40	0.09	0.03	2.23
Std D	28.95	1.50	19.30	8.40	0.29	1.27	0.92	1.84	0.41	0.02	0.37	0.53	0.01	0.01	0.87

Table 2

Mean of antioxidant consumption (%) during 4 h incubation of $PM_{2.5}$, PM_{10}, and TSP

	PM Type	%OP^{AA}		%OP^{UA}		%OP^{GSH}	
		x	±SD	x	±SD	x	±SD
$PM_{2.5}$	Indoor	34.56	3.38	5.94	1.64	1.78	4.56
	Outdoor	32.98	2.28	8.03	2.55	3.60	1.58
PM_{10}	Indoor	25.00	2.57	5.22	3.40	0.20	2.52
	Outdoor	27.75	0.95	7.55	3.35	5.08	3.15
TSP	Indoor	32.42	1.28	4.68	3.90	0.00	3.92
	Outdoor	25.70	1.22	7.52	2.96	1.78	2.38
	SP^{a}_{blank}	6.90	1.40	4.60	3.50	2.30	4.00
LDN^{b}		57.40	1.90	3.10	5.50	31.90	0.50

Results are shown for ascorbate oxidation (expressed as OP^{AA}), glutathione oxidation (expressed as OP^{GSH}), and urate oxidation (expressed as OP^{UA})

[a] Filter blank

[b] London roadside PM Control

Table 3

The ascorbate oxidation (expressed as OP^{AA} μg^{-1} or OP^{AA} m^{-3}), urate oxidation (expressed as OP^{UA} μg^{-1}), and glutathione oxidation (expressed as OP^{GSH} μg^{-1}) broken down into indoor and outdoor collection sites

	PM type	OP^{AA} μg^{-1} PM		OP^{AA} m^{-3}		OP^{UA} μg^{-1} PM[a]		OP^{GSH} μg^{-1} PM[a]	
		x	±SD	x	±SD	x	±SD	x	±SD
$PM_{2.5}$	Indoor	1.16	0.14	4825.28	392.52	0.12	0.06	−0.04	0.18
	Outdoor	1.05	0.10	319.73	8.95	0.13	0.10	0.05	0.05
PM_{10}	Indoor	0.88	0.10	20,181.90	3003.25	0.15	0.15	−0.05	0.10
	Outdoor	0.85	0.03	3090.70	202.78	0.13	0.15	0.15	0.13
TSP	Indoor	1.18	0.04	149,358.66	5600.50	0.14	0.16	−0.06	0.14
	Outdoor	0.76	0.06	15,143.30	1254.23	0.12	0.12	−0.02	0.10
LDN[b]	Outdoor	2.20	0.10	5.32[c]	4.52	0.10	0.20	1.30	0.00

[a] The OP^{UA} μg^{-1} and OP^{GSH} μg^{-1} were calculated to be less than the minimum detection value of 0.2 based on a minimum measurable % OP of 10% and will not be reported further

[b] London roadside PM Control

[c] Godri et al. (2011)